Large-scale simulation of interictal epileptic discharges with neural mass models: patient specific interpretation of the interictal SEEG data

Elif Köksal-Ersöz, Julia Makhalova, Maxime Yochum, Christian-G Bénar, Maxime Guye, Fabrice Bartolomei, Fabrice Wendling, Isabelle Merlet

Large-scale simulation of interictal epileptic discharges with neural mass models: patient specific interpretation of the interictal SEEG data

Elif Köksal-Ersöz[1], Julia Makhalova[2, 3], Maxime Yochum[1], Christian-G. Bénar[3, 4], Maxime Guye[5], Fabrice Bartolomei [2,4], Fabrice Wendling[1], Isabelle Merlet[1]

1 Univ Rennes, INSERM, LTSI - UMR 1099, Rennes, France

2 Assistance Publique—Hôpitaux de Marseille, Service d'Épileptologie et de Rythmologie Cérébrale, Hôpital La Timone, Marseille, France

3 Aix Marseille Univ, CNRS, CRMBM UMR 7339, Marseille, France

4 Institut de Neurosciences des Systèmes (INS, UMR 1106), Aix Marseille Université, INSERM, Marseille, France

5 APHM, Hôpital de la Timone, CEMEREM, Marseille, France

Corresponding authors:
Elif Köksal-Ersöz
LTSI INSERM U1099 - Université de Rennes
Campus de Beaulieu - Batiment 22
35042 Rennes Cedex, FRANCE
elif.koksal-ersoz@inserm.fr
Orcid: 0000-0003-3696-7953

Isabelle Merlet
LTSI INSERM U1099 - Université de Rennes
Campus de Beaulieu - Batiment 22
35042 Rennes Cedex, FRANCE
isabelle.merlet@inserm.fr
Orcid: 0000-0003-2590-6848

Abstract

In patients with refractory epilepsy, the clinical interpretation of stereoelectroencephalographic (SEEG) signals is crucial to delineate the epileptogenic network that should be targeted by surgery. We propose a pipeline of patient-specific computational modeling of interictal epileptic activity to improve the definition of regions of interest. Comparison between the computationally defined regions of interest and the resected region confirmed the efficiency of the pipeline. This result suggests that computational modeling can be used to reconstruct signals and aid clinical interpretation.

Key words: drug-resistant epilepsy, interictal epileptic discharge, inverse problem, SEEG modeling, neural mass models

Abbreviations: SEEG: Stereoelectroencephalography. IED: interictal epileptic discharge. ROI: region of interest. MRI: magnetic resonance imaging. FCD: focal cortical dysplasia. CT: computed tomography. VEP: virtual epileptic patient. DW-MRI: diffusion-weighted MRI. wMNE: weighted minimum-norm estimation. NMM: neural mass model. BEM: boundary element method. FEM: finite element method.

Introduction

Stereoelectroencephalographic (SEEG) signals recorded in patients with drug-resistant focal epilepsy show distinct activity patterns during interictal, preictal, and ictal periods. These patterns are analyzed to define the epileptogenic zone and propagation zone networks [1]. Although recorded within epileptic tissue, SEEG signals reflect the projection of epileptic activity from multiple sources onto the multiple contacts of the intracerebral electrode, which complicates their visual interpretation. Previous studies have suggested that computational modeling of source activity can improve the source localization problem of transcranial recordings [2, 3].

This short communication is a proof of concept illustrating that patient specific modeling of head anatomy and source activity with a neurophysiologically plausible model combined with source localization can improve the interpretation of SEEG recorded interictal epileptic discharges (IEDs), and provide additional information to the clinical interpretation of SEEG signals. Results suggest that patient specific modeling can refine the definition of the Region Of Interest (ROI) responsible for IEDs.

Methods

Patient data

The patient was a 14–year-old right-handed girl diagnosed with left occipital, MRI (magnetic resonance imaging)-negative focal cortical dysplasia (FCD). The patient underwent a presurgical evaluation at the epilepsy unit of La Timone Hospital, Marseille, France. MRI acquisitions were performed according to the procedure described elsewhere [4]. Thirteen SEEG electrodes were

placed (Alcis, 10–18 contacts with length 2 mm, diameter 0.8 mm, spaced by 1.5 mm). Electrode positions were verified by computed tomography (CT) scan. Signals were recorded on a Natus system at a sampling rate of 1024 Hz.

The epileptogenic zone network defined by expert clinicians (FB, JM) was located within the left lateral (O2) and polar occipital cortex (contacts GL'4-8) where the ictal and interictal epileptic activity was recorded. Surgery was restricted to the resection of the lateral part of the epileptogenic zone (contacts GL'6-8) due to the functional constraints and led to significant improvement of the epilepsy (rare disabling seizures, Engel class II).

Simulation of SEEG signals on the whole brain model

The patient-specific modeling pipeline (Figure 1) includes construction of the head model and simulation of the source activity.

For the construction of the head model, the MRI data were segmented using FreeSurfer [5]. The resulting cortical mesh was imported to Brainstorm [6], and downsampled to 15000 vertices. The neocortex was then subdivided into 144 regions according to the Virtual Epileptic Patient (VEP) atlas [7]. Streamline tractography from diffusion-weighted MRI (DW-MRI) was used to estimate structural connectivity and delay matrices [4].

IEDs were detected visually from the patient's SEEG data. The weighted minimum-norm estimation (wMNE) method was used to localize the source activity. The source activity was simulated by using a layered neural mass model (NMM) of the neocortex [8]. Each region of the brain atlas was associated with an NMMs interconnected via the structural connectivity and

delay matrices. The parameters of the NMMs were identified to fit either the averaged IED morphology observed in the real SEEG recordings or the background activity [8].

The forward problem was solved by considering the *extended* source activity. Briefly, a given brain region contained *N* vertices, each of which was associated with an elementary dipole. The same source activity was assigned to all vertices within the brain region associated with an NMM. An active (i.e. epileptic) ROI contained dipoles assigned with the source activity signals that simulate IED. The dipoles of an inactive (i.e. non-epileptic) region were assigned with source activity signals simulating background activity. The simulated source activity defined the extended source matrix S of 15000 x T, with *T* being the size of the time vector of the simulated activity. A lead field matrix, A (117 x 15000), generated from a 1-layer Boundary Element Method (BEM) model [9], was used to compute the projection of the source activity onto the SEEG electrodes. The X (117 x *T*) matrix of simulated SEEG signals was obtained by X=A.S. The agreement between the simulated and recoded signals was measured with the agreement of polarity inversions at the level bipolar contacts.

Results

Two distinct types of IEDs were detected visually on different SEEG contacts. The first type of IED was a spike involving the GL'5-GL'6 contacts, and was preceded 10 ms by a brief spike with the same polarity on the GL'4-GL'5 contacts (Figure 2A). A polarity inversion was observed between the contacts GL'5-GL'6 and GL'6-GL'7. The spike activity was localized from an average of 20 IEDs by the wMNE in the left lateral occipital and in the left lingual sulcus (basal occipital cortex). The SEEG simulated from the source activities assigned to the wMNE-defined ROIs showed the largest component on GL'4-GL'5 but with a polarity inversion

on adjacent contacts (Figure 2B). The wMNE-defined ROIs were re-delineated by downsizing the one in the left sulcus and by downsizing the one in the left lateral occipital but adding regions which were not included by the wMNE. The new simulated signal showed the same polarity inversion as in the real SEEG, with a 10 ms difference between the events (Figure 2C).

The second type of IED was a spike-wave with maximal spike amplitude on GL'2-GL'3 and a discrete polarity inversion on adjacent contacts during the first peak of the spike-wave. The transient activity on GL'1-GL'2 preceded the spike-and-wave by 10 ms. The wMNE solution obtained from an average of 20 IEDs was located in the left medial occipital region (lingual gyrus). The SEEG signal simulated by assigning the source activity to the wMNE-defined ROI yielded a maximal spike amplitude on GL'1-GL'2 (Figure 2E). We optimized the ROI by enlarging the wMNE-defined ROI and dividing it into two (one small ROI is surrounded by a larger ROI). We associated distinct source activities to each region. The new simulated signal showed the maximal spike amplitude on GL'2-GL'3, followed the correct polarity inversions on adjacent contacts and the time difference (Figure 2F).

The surgically resected zone corresponding to the left lateral occipital (Figure 2B-F) covered only one of the three regions defined by the model. It is worth mentioning that the surgical resection targeted the clinically defined epileptogenic zone network, which did not include the lingual gyrus and the lingual sulcus. Despite the presence of IEDs, these medial occipital regions were considered by clinicians as a part of the propagation zone.

Discussion

We presented a pipeline to define cortical ROIs responsible for IED generation by combining SEEG source localization, realistic source modeling, and SEEG forward solution in a patient-specific anatomical model. The source localization from intracerebral recordings is refined by using a computational model that can finely simulate IEDs respecting the polarity inversions on SEEG electrodes, which are determinant for the localization of epileptogenic regions.

In the present case, there was also an incomplete concordance between the clinically defined epileptogenic regions and the IED-generating regions simulated by the model. This is not surprising given that the concordance between the regions showing maximal interictal spiking activity and those with maximal epileptogenicity is known to be incomplete in about 25% of patients with FCD [10]. Nonetheless, one of three IED-generating regions identified by the model corresponded perfectly with the resected epileptogenic zone, thus validating our pipeline. The other two regions spared by the resection might correspond to the remaining epileptogenic regions responsible for the persisting seizures.

Our method of ROI localization is based on matching IED morphology and polarity inversion of recorded and simulated signals, for which the patch location and its size were also crucial. Modeling IED morphologies allows to decipher the pathophysiological mechanisms mediating IEDs, which can be of clinical relevance [11] and adds information to ictal analysis. The manual estimation of the model parameters and patches is currently a limitation, which can be overcome by the development of an automatic model fitting pipeline. The overall framework can be adapted to train artificial neural networks for improving SEEG source imaging, as suggested for transcranial imaging techniques [12].

We considered a BEM based three-layer homogeneous isotropic head model. Solving the inverse problem using a finite element method (FEM) based five-layer homogeneous isotropic head model gave similar results to those obtained with the BEM. However, the FEM forward solution could not be performed as it would imply using volumes of interest instead of ROIs, as well as, a volumic parcellation of the brain atlas. Finally, the FCD subtypes present specific and distinct alternations of neuronal populations, as well as the architectural and cytoarchitectural abnormalities of cortical layers [13, 14]. Such pathophysiological abnormalities are uneasy to model, and might be the current limitation for proposing a more specific modeling approach integrating the underlying etiology.

To conclude, this study suggests that a combination of anatomical and computational models can be successfully used to guide the localization of epileptogenic regions. Although further validation in a large patient cohort is mandatory, this modeling approach is particularly relevant for designing surgical interventions and neuromodulation protocols.

Funding Sources

This project has received funding from the European Research Council (ERC) under the European Union's Horizon 2020 research and innovation program (grant agreement No 855109).

Ethics approval

This data subset is a part of the dataset of the project named "EEG-Process" ("Retrospective analysis of EEG signals collected in routine care during the evaluation of epileptic patients") which was approved by legal entities including the Institutional Review Board (IRB00003888,

IORG0003254, FWA00005831) of the French Research Institute for Health and Medical Research (INSERM).

Disclosure of Conflict of Interest

None of the authors has any conflict of interest to disclose.

Data availability statement

The data that support the findings of this study are available from the corresponding author upon reasonable request, subject to privacy and ethical restrictions as appropriate.

Author Contributions

EKE and IM conceived and designed the study. EKE performed modeling and numerical simulation. EKE and MY designed the simulation platform. JM and MG helped in the acquisition and analysis of the data. JM, FB, C-GB and IM analyzed and interpreted the clinical data. EKE and IM drafted the manuscript. All authors contributed to revising the manuscript.

References

1. Bartolomei F, Lagarde S, Wendling F, McGonigal A, Jirsa V, Guye M, et al. Defining epileptogenic networks: Contribution of SEEG and signal analysis. Epilepsia. 2017;58(7):1131–47.

2. Cosandier-Rimele D, Badier J-M, Chauvel P and Wendling F. A Physiologically Plausible Spatio-Temporal Model for EEG Signals Recorded With Intracerebral Electrodes in Human Partial Epilepsy. IEEE Transactions on Biomedical Engineering 2007; 54: 380–8.
3. Chowdhury RA, Lina JM, Kobayashi E, Grova C. MEG Source Localization of Spatially Extended Generators of Epileptic Activity: Comparing Entropic and Hierarchical Bayesian Approaches. PLOS ONE. 2013;8(2):e55969.
4. Besson P, Bandt SK, Proix T, Lagarde S, Jirsa VK, Ranjeva JP, et al. Anatomic consistencies across epilepsies: a stereotactic-EEG informed high-resolution structural connectivity study. Brain. 2017; 140(10):2639–52.
5. Dale AM, Fischl B, Sereno MI, Cortical surface-based analysis. I. Segmentation and surface reconstruction. Neuroimage, 1999; 9:179-194.
6. Tadel F, Baillet S, Mosher JC, Pantazis D, Leahy RM. Brainstorm: A User-Friendly Application for MEG/EEG Analysis. Computational Intelligence and Neuroscience. 2011; 2011:879716.
7. Wang HE, Scholly J, Triebkorn P, Sip V, MedinaVillalon S, Woodman MM, et al. VEP atlas: An anatomic and functionalhuman brain atlas dedicated to epilepsy patients. Journal of Neuroscience Methods. 2020; 348:108983.
8. Köksal-Ersöz E, Lazazzera R, Yochum M, Merlet I, Makhalova J, Mercadal B, et al.. Signal processing and computational modeling for interpretation of SEEG-recorded interictal epileptiform discharges in epileptogenic and non-epileptogenic zones. Journal of Neural Engineering 2022; 19:055005.

9. Bensaid S, Modolo J, Merlet I, Wendling F and Benquet P. COALIA: A Computational Model of Human EEG for Consciousness Research. Frontiers in System Neuroscience 2019; 13.
10. Bartolomei F, Trébuchon A, Bonini F, Lambert I, Gavaret M, Woodman M, et al. What is the concordance between the seizure onset zone and the irritative zone? A SEEG quantified study. Clinical Neurophysiology. 2016; 127(2):1157–62.
11. de Curtis M, Jefferys JGR, Avoli M. Interictal Epileptiform Discharges in Partial Epilepsy: Complex Neurobiological Mechanisms Based on Experimental and Clinical Evidence. In: Noebels JL, Avoli M, Rogawski MA, et al., editors. Jasper's Basic Mechanisms of the Epilepsies [Internet]. 4th edition. Bethesda (MD): National Center for Biotechnology Information (US); 2012. Available from: https://www.ncbi.nlm.nih.gov/books/NBK98179/
12. Sun R, Sohrabpour A, Worrell G A and He B. Deep neural networks constrained by neural mass models improve electrophysiological source imaging of spatiotemporal brain dynamics. Proceedings of the National Academy of Sciences 2022; 119:e2201128119.
13. Medici V, Rossini L, Deleo F, Tringali G, Tassi L, Cardinale F, et al. Different parvalbumin and GABA expression in human epileptogenic focal cortical dysplasia. Epilepsia. 2016; 57(7):1109–19.
14. Lagarde S, Scholly J, Popa I, Valenti-Hirsch MP, Trebuchon A, McGonigal A, et al. Can histologically normal epileptogenic zone share common electrophysiological phenotypes with focal cortical dysplasia? SEEG-based study in MRI-negative epileptic patients. J Neurol. 2019; 266(8):1907–18.

Figures

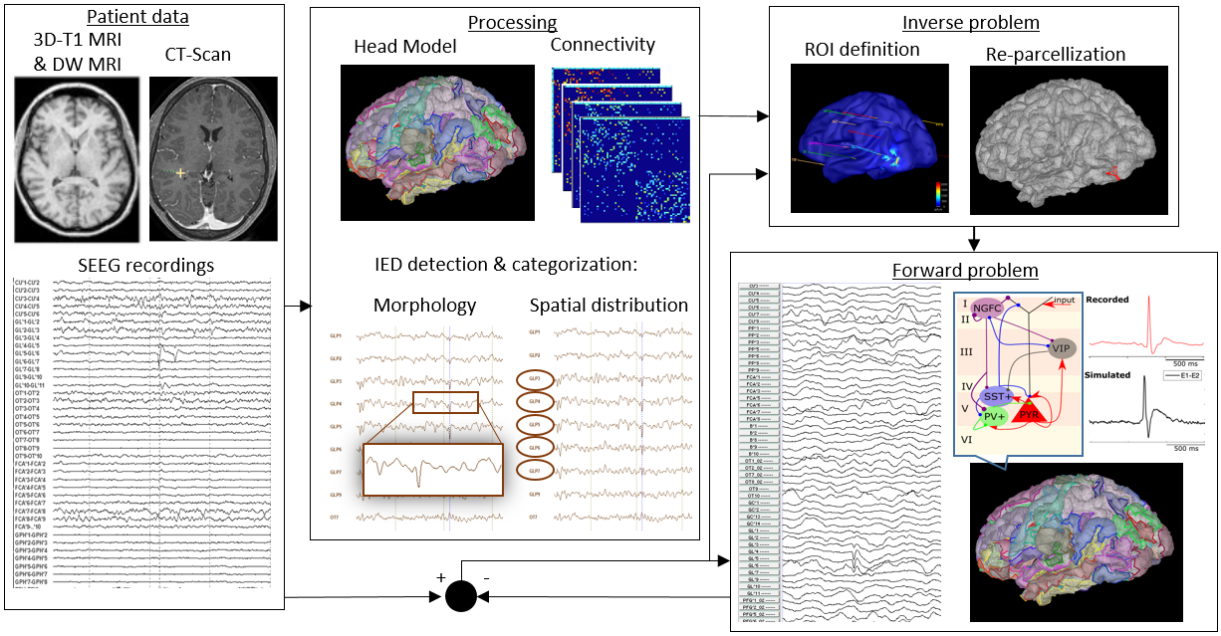

Figure 1. Pipeline for patient specific intracerebral IED simulation. Patient data including 3D-T1 MRI, DW MRI, CT-scan and SEEG recordings are processed for patient specific head modeling, connectivity matrix, IED detection and categorization. Following the solution to the inverse problem, ROIs were defined and inserted into the atlas. SEEG signals were simulated using a cortical neural mass model. An iterative process of redefining ROIs and improving the SEEG morphology was performed to reduce the difference between the real and simulated SEEG signals.

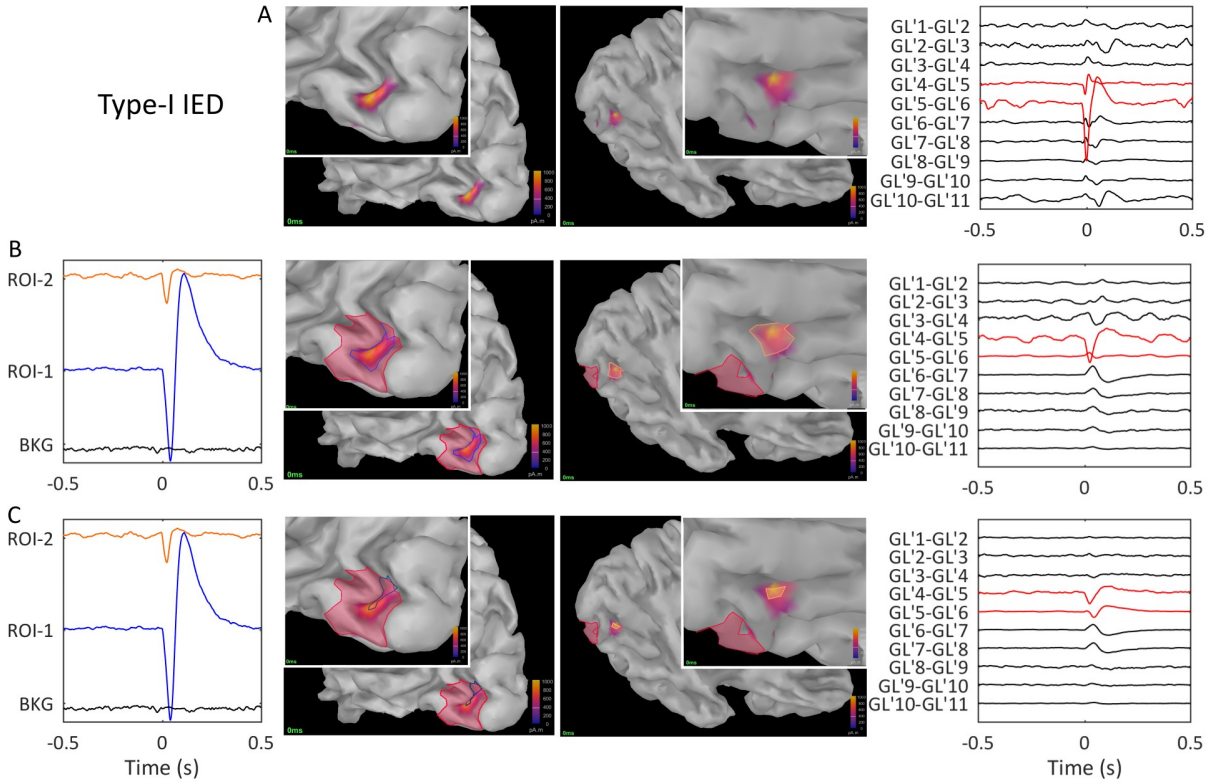
A
Type-I IED
B
ROI-2
ROI-1
BKG
C
ROI-2
ROI-1
BKG
-0.5
0
0.5
Time (s)
GL'1-GL'2
GL'2-GL'3
GL'3-GL'4
GL'4-GL'5
GL'5-GL'6
GL'6-GL'7
GL'7-GL'8
GL'8-GL'9
GL'9-GL'10
GL'10-GL'11
0ms

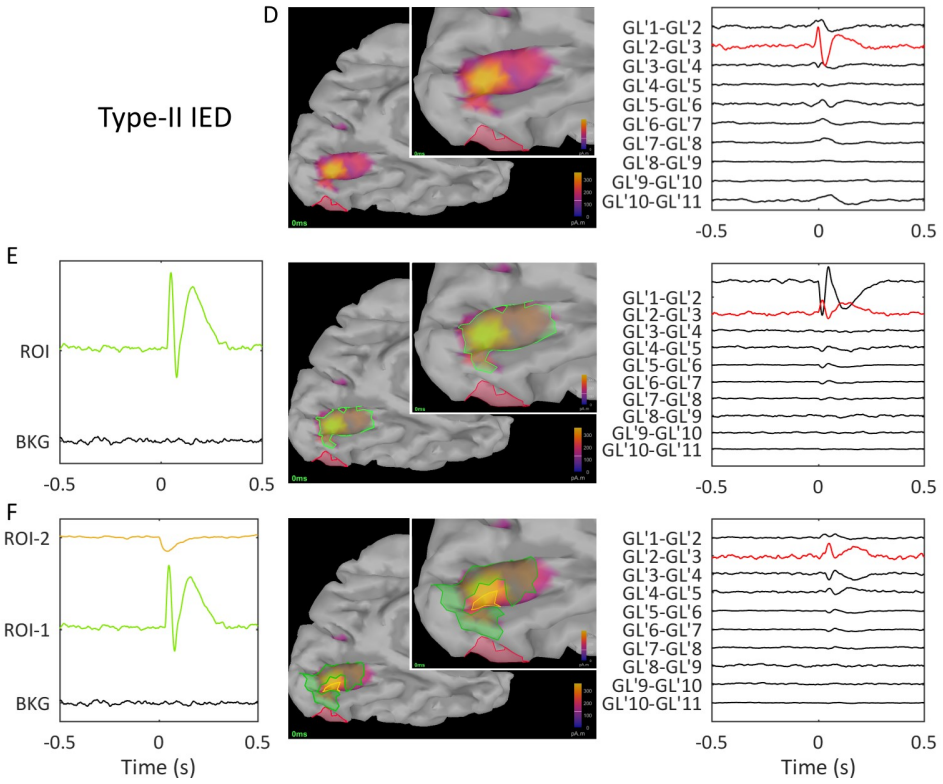
D
Type-II IED
E
ROI
BKG
F
ROI-2
ROI-1
BKG
-0.5
0
0.5
Time (s)
GL'1-GL'2
GL'2-GL'3
GL'3-GL'4
GL'4-GL'5
GL'5-GL'6
GL'6-GL'7
GL'7-GL'8
GL'8-GL'9
GL'9-GL'10
GL'10-GL'11
0ms

Figure 2 Two distinct types of IEDs were detected on the GL' electrode. (A) Type-I IED localized in the left lateral occipital (O2) and left lingual sulcus by the wMNE method showed a biphasic spike morphology (right panel). (B) Simulated source activities for the active ROIs (ROI-1 and ROI-2 signals on the left panel) were assigned for the regions defined by the wMNE method, i.e. ROI-1 for the left O2 (blue region) and ROI-2 for the left lingual sulcus (orange region) (middle panels). The source activities were triggered by a brief pulse stimulation with a 10 ms delay to capture the observed temporal difference between the GL'4-GL'5 and GL'5-GL'6 SEEG signals in (A). The background (BKG) source activity was assigned to the inactive regions. The simulated SEEG showed the largest component on GL'4-GL'5 with an inversion of polarity on GL'5-GL'6 and a 10 ms difference between the signals on GL'5-GL'6 and GL'6-GL'7 (right panel). (C) The same source activities for the active and inactive regions were associated with the manually optimized ROIs (middle panels). The new simulated SEEG showed the same polarity on GL'4-GL'5 and GL'5-GL'6 with a 10 ms difference between the peaks and a polarity inversion between GL'5-GL'6 and GL'6-GL'7 (right panel). (D) Type-II IED localized in the left lingual gyrus by the wMNE method showed a spike-and-wave morphology (right panel). (E) Simulated source activities for the active ROI (ROI signal on the left panel) were assigned for the ROI (green patch on the middle panel) defined by the wMNE method. The source activity was triggered by a brief pulse stimulation. The background (BKG) source activity was assigned to the inactive regions. The simulated SEEG showed the largest component on GL'1-GL'2 with an inversion of polarity on GL'2-GL'4. No activity appeared on GL'3-GL'4 contacts (right panel). (F) The wMNE-derived ROI was optimized by defining a small ROI (ROI-1, yellow patch) and a larger ROI (ROI-2, green patch) (middle panels). A source signal of spike-and-wave morphology was associated with ROI-2 (green ROI-2 signal on the left panel). A

source signal that appeared 10 ms before the main spike-and-wave was associated with ROI-1 (yellow ROI-1 signal on the left panel). The source activities were triggered by a brief pulse stimulation. The new simulated SEEG followed the inverted polarities on GL'1-GL'2, GL'2-GL'3, and GL'3-GL'4, as well as the 10 ms time difference during the initial phase of the SEEG signals on GL'1-GL'2 and GL'2-GL'3 (right panel). Red zones delineated in (B), (C), (E), and (F) show the resected zone in the surgery. Insets zoom into the active regions of interest.